Journal of Chromatography A 1614 (2020) 460737

Contents lists available at ScienceDirect

Journal of Chromatography A

journal homepage: www.elsevier.com/locate/chroma

Peak focusing based on stationary phase thickness gradient

Maxwell Wei-Hao Li[a,b,c], Hongbo Zhu[a,b], Menglian Zhou[a,b], Jinyan She[a,b], Ziqi Li[a,d], Katsuo Kurabayashi[b,e], Xudong Fan[a,b,*]

[a] Department of Biomedical Engineering, University of Michigan, Ann Arbor, MI 48109, USA
[b] Center for Wireless Integrated MicroSensing and Systems (WIMS2), University of Michigan, Ann Arbor, MI 48109, USA
[c] Department of Electrical Engineering and Computer Science, University of Michigan, Ann Arbor, MI 48109, USA
[d] School of Precision Instruments and Opto-electronics Engineering, Tianjin University, PR China
[e] Department of Mechanical Engineering, University of Michigan, Ann Arbor, MI 48109, USA

ARTICLE INFO

Article history:
Received 30 September 2019
Revised 24 November 2019
Accepted 25 November 2019
Available online 26 November 2019

Keywords:
Gas chromatography
Stationary phase gradient
Thickness gradient
Peak focusing
Resolution
Peak capacity

ABSTRACT

This paper reports the development of a stationary phase thickness gradient gas chromatography (GC) column that enables analyte peak focusing and improves separation resolution. Theoretical analysis and simulation demonstrate focusing via a positive thickness gradient, *i.e.*, the stationary phase thickness increases along the column. This effect was experimentally verified by coating a 5 m long capillary column with a film thickness varying from 34 nm at the column inlet to 241 nm at the column outlet. The column was analyzed in forward (thin to thick) and backward (thick to thin) modes and compared to a uniform thickness column with a thickness of 131 nm, using alkanes ranging from C_5 to C_{16} and aromatics. Comparison of resolutions between forward mode and the uniform thickness column demonstrated an overall focusing rate (*i.e.*, improvement in peak capacity) of 11.7% on alkanes and 28.2% on aromatics. The focusing effect was also demonstrated for isothermal room temperature separation of highly volatile compounds and temperature programmed separation with different ramping rates. In all cases, peak capacities from forward mode separations are higher than those from other modes, indicating the ability of a positive thickness gradient to focus analyte peaks. This thickness gradient technique can therefore be broadly applied to various stationary phases and column types as a general method for improving GC separation performance.

1. Introduction

Gas chromatography (GC) is an analytical method for separating gas phase compounds via separation columns, allowing for analysis and identification of compounds in a target sample. In wall coated capillary columns, vapor interactions between the gas phase and a stationary phase coated on a capillary wall allow for retention of analytes. As analytes travel along the column, they encounter longitudinal and transverse mass transfer, which results in peak broadening, decreasing GC resolution and increasing the possibility of co-elution. Typically, proper selection of the column stationary phase (to allow for sufficient analyte interaction and retention) [1–4], application of temperature-programmed profiles [5–7], and split/splitless sample injection [5] allow for improvement of chromatograph separation and resolution. In some cases, however, these methods are insufficient to achieve a desired separation; for example, in portable GC, limited carrier gas supplies prevent use of split injections, while fine control over temperature programming is both difficult and limited by system power capacity [8,9]. Furthermore, even for specialized separations (e.g., separation of highly volatile compounds by porous layer open tubular columns [2,10,11]), it can be difficult to fully separate the complete range of relevant compounds. An additional method for improving column separation is therefore desirable.

Negative temperature gradient separation (NTGS) [12] is one method that has been shown to improve column performance by sharpening elution peaks [13–19]. In NTGS, the column inlet is heated, and a temperature gradient is generated via thermal exchange with the ambient environment. Since the temperature is lower toward the column outlet, the peak front travels more slowly than its tail, resulting in overall peak focusing. This effect can be optimized by tuning different temperature profiles along the column, allowing for high versatility under different conditions [12–19]. However, due to NTGS reliance on thermal exchange, focusing varies with ambient temperature, humidity, air convection rate, and packing material thermal conductivity, reducing repeatability

* Corresponding author at: Department of Biomedical Engineering, University of Michigan, Ann Arbor, MI 48109, USA.
E-mail address: xsfan@umich.edu (X. Fan).

https://doi.org/10.1016/j.chroma.2019.460737
0021-9673/

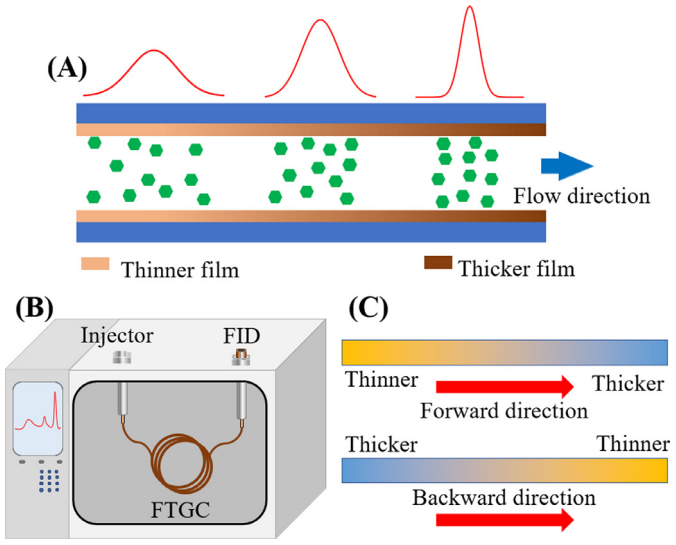

Fig. 1. (A) Depiction of peak focusing by FTGC. A thinner to thicker film focuses an analyte peak as it travels along the column. (B) Setup for column performance evaluation. The column was installed in an Agilent 6890 benchtop GC equipped with a flame ionization detector. (C) Illustration of forward and backward modes. Columns were tested in one direction first, then reversed. Comparisons are made between chromatograms obtained from the two modes.

and predictability (especially if complex temperature profiles are used). Sophisticated heat control modules can be used to stabilize the temperature gradient, but add additional size, weight, complexity, and cost to the GC device. Additionally, energy loss due to the aforementioned thermal exchange is a relevant detriment for systems with limited resources (*e.g.*, micro GC devices). Furthermore, separation of high volatility compounds often requires near ambient temperatures, which disallows generation of a temperature gradient and thus inhibits the NTGS effect. Therefore, although versatile and tunable, NTGS usage for certain applications (*e.g.*, portable GC) may be limited and challenging.

This paper proposes an alternative method for peak focusing via a positive stationary phase thickness gradient (*i.e.*, increased film thickness toward the outlet), as illustrated in Fig. 1(A). With the increased stationary phase thickness toward the outlet, the peak front travels more slowly than its tail, resulting in overall peak focusing. Herein, theory and simulation are first provided to explain underlying focusing mechanisms. Subsequently, the peak focusing effect is experimentally demonstrated by using a 5 m long film thickness gradient column (FTGC) created from a deactivated capillary column dynamically coated with a 5% phenyl stationary phase. Four sets of experiments are performed to characterize the FTGC's peak focusing abilities. An overall focusing rate of up to 28.2% was observed. Focusing of high volatility compounds at room temperature was also achieved.

2. Peak focusing theory

A theoretical explanation for peak focusing is provided in this section. Detailed simulation will be presented in the next section.

The effective velocity, $u_{eff}(x,t)$, of an analyte at a location x (the distance from the column inlet) and a given time t is given by

$$u_{eff}(x,t) = \frac{u_M(x,t)}{1+k(x,t)}, \tag{1}$$

where $u_M(x,t)$ is the velocity of the mobile phase and $k(x,t)$ is the retention factor:

$$k(x,t) = \frac{K(x,t)}{\beta(x)}, \tag{2}$$

with distribution coefficient $K(t)$ defined as

$$K(x,t) = \exp\left(\frac{\Delta G}{RT(x,t)}\right), \tag{3}$$

where R is the universal gas constant and $T(x,t)$ is the time dependent column temperature at location x. ΔG is the Gibbs free energy change associated with an analyte moving from the stationary to mobile phase and can be calculated from the change in analyte enthalpy (ΔH) and entropy (ΔS)

$$\Delta G = \Delta H - T\Delta S. \tag{4}$$

The phase ratio β is defined by

$$\beta = \frac{\left(d_i - 2d_f\right)^2}{d_i^2 - \left(d_i - 2d_f\right)^2} \approx \frac{d_i}{4d_f}, \quad for\ d_i \gg d_f \tag{5}$$

where d_i and $d_f(x)$ are the column inner diameter and the film thickness, respectively. Eq. (2) can thus be expressed as

$$k(x,t) = A\exp\left(\frac{\Delta G}{RT(x,t)}\right) \times d_f(x), \tag{6}$$

where A is a constant for a given column. The retention factor change along the column, $\delta k(x,t)$, can be written as (see derivation in Supporting Information)

$$\frac{\delta k(x,t)/\delta x}{k(x,t)} = -\frac{\Delta H}{RT(x,t)}\frac{\delta T(x,t)/\delta x}{T(x,t)} + \frac{\delta d_f(x)/\delta x}{d_f(x)}. \tag{7}$$

Eq. (7) shows that the fractional increase of the retention factor, $\delta k/k$, along the column in distance δx has two contributions: a negative temperature gradient given by the first term and a positive film thickness gradient given by the second term. This retention factor gradient ($\delta k/k$) is related to a velocity gradient by Eq. (1); thus, both a negative temperature gradient and a positive film thickness gradient result in a velocity difference between the front and tail of a band, allowing for band focusing (i.e., the spatial distribution of an analyte experiences a spatially varying velocity gradient). At the outlet, the band is observed as a time varying peak during elution, which can be narrower than the corresponding peak from an unfocused band. In other words, peak focusing (an observable quantity) occurs as a result of band focusing within the column. The equivalency of these two gradients can be expressed as

$$-\frac{\Delta H}{RT(x,t)}\frac{\delta T(x,t)}{T(x,t)} = \frac{\delta d_f(x)}{d_f(x)}. \tag{8}$$

Fig. S1 plots the equivalent temperature gradient for C_{10} for various fractional film thickness gradients and column temperatures based on Eq. (8). Figure S2 shows the equivalent temperature gradient for C_{10}, C_{12}, and C_{14} at various temperatures and a fractional film thickness gradient of 50%.

The film thickness gradient has several advantages over temperature gradient-based peak focusing. First, the film thickness gradient is independent of column temperature, allowing for focusing of analytes of any volatilities at any operation temperatures. High volatility compounds, especially, are difficult to focus with NTGS, but can be accomplished with an FTGC. Second, while the temperature gradient may vary with heater and ambient conditions (such as heater arrangement, heat dissipation, column size/weight, column channel arrangement, and ambient temperature and air flow), the film thickness gradient is always constant and allows for more reliable and repeatable GC operation (less susceptible to environmental effects). Finally, the FTGC can be used without extra accessories (such as heaters or coolers, which are required for NTGS), which significantly reduces device complexity for future integration. However, despite these advantages, film thickness gradient

based separation is less versatile than NTGS since the gradient is fixed, whereas a temperature gradient can be adjusted by changing the heat source and/or drain. In addition, the increased film thickness toward the column outlet may result in slower mass transfer, potentially offsetting the peak focusing effect. The mass transfer effect is examined in the following simulation.

3. Simulation

For this simulation, no temperature gradient (i.e., NTGS) is considered; only a film thickness gradient is analyzed. The time dependent concentration c of an analyte peak traveling along a column is determined by solving the transient convection-diffusion equation [20]

$$\frac{\partial c}{\partial t} = -\frac{\partial}{\partial x}\left(u_{eff}c\right) + \frac{\partial}{\partial x}\left(D_{eff}\frac{\partial c}{\partial x}\right), \tag{9}$$

where $u_{eff}(x,\ t)$ is given in Eq. (1). The effective diffusion, D_{eff}, can be calculated from local dispersion, D, and the retention factor $k(x,t)$

$$D_{eff}(x,t) = \frac{D(x,t)}{1+k(x,t)}, \tag{10}$$

$$D = D_M(x,t) + \frac{1}{2}\left[\frac{1+6k(x,t)+11k(x,t)^2}{24(1+k(x,t))^2}\frac{d_i^2}{D_M(x,t)} + \frac{2k(x,t)}{3(1+k(x,t))^2}\frac{d_f(x,t)^2}{D_S(x,t)}\right]u_M(x,t)^2, \tag{11}$$

with d_f as the film thickness and D_M as the mobile phase diffusion constant. Note that D includes both longitudinal and transverse mass transfer/diffusion. $D_M(x,t)$ can be expressed as

$$D_M(x,t) = D_C\frac{T(t)^{1.75}}{p(x)} = 5\ \times 10^4 D_S(x,t), \tag{12}$$

with diffusion constant D_C (dependent on molar weights and atomic and structural diffusion volumes of analytes and mobile phase molecules) and D_S as the stationary phase diffusion constant [20]. Local pressure $p(x)$ is determined from inlet and outlet pressures p_{in} and p_{out}

$$p(x) = \sqrt{p_{in}^2 - \left(p_{in}^2 - p_{out}^2\right)\frac{x}{L}} \tag{13}$$

with L being the length of the column. u_M, the velocity in mobile phase is given by

$$u_M(x,t) = \frac{d_i^2}{16\eta(t)L}\frac{1}{p(x)}\left(p_{in}^2 - p_{out}^2\right), \tag{14}$$

with viscosity η provided as a function of reference viscosity η_0 at temperature T_0 and gas type dependent exponent α_n:

$$\eta(t) = \eta_0\left(\frac{T(t)}{T_0}\right)^{\alpha_n}. \tag{15}$$

In Eq. (12), note that temperature $T(x,t)$ is provided as $T(t)$ under the assumption that the temperature remains the same along the column at a given time t. Eq. (9) can be solved by applying a finite difference model to discrete time (t) and position (i) vectors

$$\frac{\partial c}{\partial t} \rightarrow \frac{\partial C}{\partial t} = \frac{C_{i,t+1} - C_{i,t}}{\Delta t} \tag{16}$$

$$\frac{\partial c}{\partial x} \rightarrow \frac{\partial C}{\partial x} = \frac{C_{i+1,t} - C_{i,t}}{\Delta x} \tag{17}$$

$$\frac{\partial^2 c}{\partial x^2} \rightarrow \frac{\partial^2 C}{\partial x^2} = \frac{C_{i+1,t} - 2C_{i,t} + C_{i-1,t}}{(\Delta x)^2}, \tag{18}$$

with Δx and Δt being simulation distance and time step sizes. Combining these yields

$$C_{i,t+1} = C_{i,t} + \Delta t\left(-u_{eff}(i,t)\frac{C_{i+1,t} - C_{i,t}}{\Delta x}\right) + \Delta t\left(D_{eff}(i,t)\frac{C_{i+1,t} - 2C_{i,t} + C_{i-1,t}}{(\Delta x)^2}\right). \tag{19}$$

The solution to Eq. (19) produces the time dependent movement of an analyte peak along the column.

To simulate Eq. (19), several boundary conditions must be set. First, at $t = 0$, the injected peak has a Gaussian peak shape, i.e.,

$$C(x,0) = \frac{1}{\sigma\sqrt{2\pi}}e^{-\frac{(x-3\sigma)^2}{2\sigma^2}}, \tag{20}$$

where σ is the initial dispersion. Note that the initial peak at time $t=0$ is at $x=3\sigma$. At the column inlet, after the initial injection, no additional analyte is injected into the column:

$$C(0,t) = 0. \tag{21}$$

At the column outlet, the last mesh concentration is approximately the same as the one to the left (since it cannot be calculated by Eq. (16)), i.e.,

$$C(L,t) = C(L-\Delta x, t). \tag{22}$$

Peak retention times and full widths at half maxima (FWHMs) can be measured at the column outlet (*i.e.*, $x = L$) by observing that, using Eq. (19), a spatially varying concentration is used to construct a two-dimensional concentration matrix varying with both position and time. By observing concentration along the second dimension (i.e., in time), a vector of concentration varying with time can be obtained, corresponding to a signal obtained from a detector at the outlet. The maximal value (varying with time) corresponds to the elution/retention time, and FWHMs can be measured by observing the times at which the concentration is half the peak value. Resolutions (R) between adjacent peaks can additionally be calculated using the formula

$$R = 1.18\ \times \frac{t_2 - t_1}{w_1 + w_2}, \tag{23}$$

where t_1 and t_2 are the retention times for two peaks and w_1 and w_2 are the corresponding FWHMs.

4. Experimental

4.1. Testing setup

The FTGC was installed in an Agilent 6890 benchtop GC equipped with a flame ionization detector (FID, see Fig. 1(B)). Ultra-high purity helium was used as the carrier gas. Evaluation of the peak focusing effect was performed with analytes injected from the thinner coating end (forward mode, i.e., traveling from thinner to thicker film) or thicker coating end (backward mode, i.e., traveling from thicker to thinner film), as illustrated in Fig. 1(C). A uniform thickness column (film thickness same as the averaged thickness) was also evaluated using the same setup for comparison. All experiments were performed using constant pressure temperature programming. Temperature programing methods and head pressures are provided in Table 1.

4.2. Materials

Analytical standard grade C_5 to C_{16}, benzene, toluene, ethylbenzene, o-xylene, 1,3-dichlorobenzene, nitrobenzene, and dichloromethane were purchased from Sigma-Aldrich (St. Louis, MO). Vinyl modified OV-1 (P/N 6001), and OV-17 (P/N 6017) were purchased from Ohio Valley Specialty Company (Marietta, OH).

Table 1
Temperature programming profiles and head pressures for simulation, uniform thickness control, separation of alkanes C_7–C_{16}, separation of aromatics, and separation of high volatility alkanes (C_5 and C_6).

	Initial temperature (°C)	Final temperature (°C)	Ramping rate (°C/min)	Head pressure (psi, mL/min)
Simulation	40	240	30	3.45, N/A
Uniform thickness control	60	180	30	3.45, 2.7
Alkane mixture (forward)	60	180	30	3.45, 2.7
Alkane mixture (equal time backward)	60	148	22	3.45, 2.7
Aromatics mixture (forward)	45	105	30	3.45, 2.9
Aromatics mixture (equal time backward)	45	90	20	3.45, 2.9
High volatility alkanes	26	26	0	2.20, 2.0

Dow SYLGARD™ 184 reagent B was purchased from Ellsworth Adhesive (Germantown, WI). Deactivated fused silica tubing (P/N 10010, 250 µm inner diameter) and an RTX-5 column (P/N 10205, cut to 5 m in length with 250 µm inner diameter and 0.1 µm film thickness) were purchased from Restek (Bellefonte, PA). A DB-1MS column (P/N 122-0162, cut to 5 m in length with 250 µm inner diameter and 0.25 µm film thickness) was purchased from Agilent (Santa Clara, CA). All materials were used as purchased without further purification or modification.

4.3. Column coating

OV-1 (75% w/w), OV-17 (10% w/w), and Dow SYLGARD™ 184 reagent B (15% w/w, crosslinker) were dissolved in dichloromethane to create a 2% (w/w) coating solution (effectively a 5% phenyl stationary phase). A 5 m long capillary column (250 µm i.d.) was silanized prior to coating by 8 repeated injections of hexamethyldisilazane (HMDS) vapor. Subsequently, an 80 µL coating solution was loaded into the capillary from the column inlet via a syringe pump (Fig. 2(A)). A 5-psi positive pressure was applied from the inlet to drive the coating solution towards the outlet. A negative 2-psi vacuum pressure was applied to the outlet through a 1 m dummy column (250 µm i.d.), which ensured a constant coating plug speed. During coating, the small volume of low boiling point dichloromethane evaporated rapidly under vacuum, progressively increasing the coating solution concentration, and hence the film thickness, as the coating solution plug moved from column inlet to outlet [21]. After coating, dry air was continuously flowed through the column for 2 h, followed by crosslinking at 80 °C for another 2 h and subsequent deactivation using HMDS. The column was then aged at 230 °C for 3 h under a helium flow of 0.5 mL/min. Using the same method, a column with a uniform thickness film was coated using a 1% (w/w) coating solution (same composition as above, but diluted) and applying a 5-psi positive pressure from the inlet to drive the coating solution toward the outlet (without applying a vacuum).

4.4. Simulation setup

Simulation of separation of C_8–C_{15} in forward and backward modes as well as using a uniform thickness equivalent to the average gradient film thickness was performed (separation conditions in Table 1). The film thickness varied from 34 nm to 241 nm for a 5 m column (inlet to outlet for forward mode and vice versa for backward mode, see Stationary phase characterization in Results and Discussion). Additional simulation parameters for C_8–C_{15} interactions with the stationary phase are provided in Tables S2 and S3 [22]. Note that calculation of retention factor $k(x,t)$ requires a value for distribution coefficient $K(t)$ (Eq. (2)), which is estimated based on values in Ref. [22] (see Section S3 – Simulation parameters and results in Supporting Information). Simulated retention times and FWHMs are provided in Table 2 and resolutions are provided in Table 3. Analysis is provided in Section 5 – Results and Discussion.

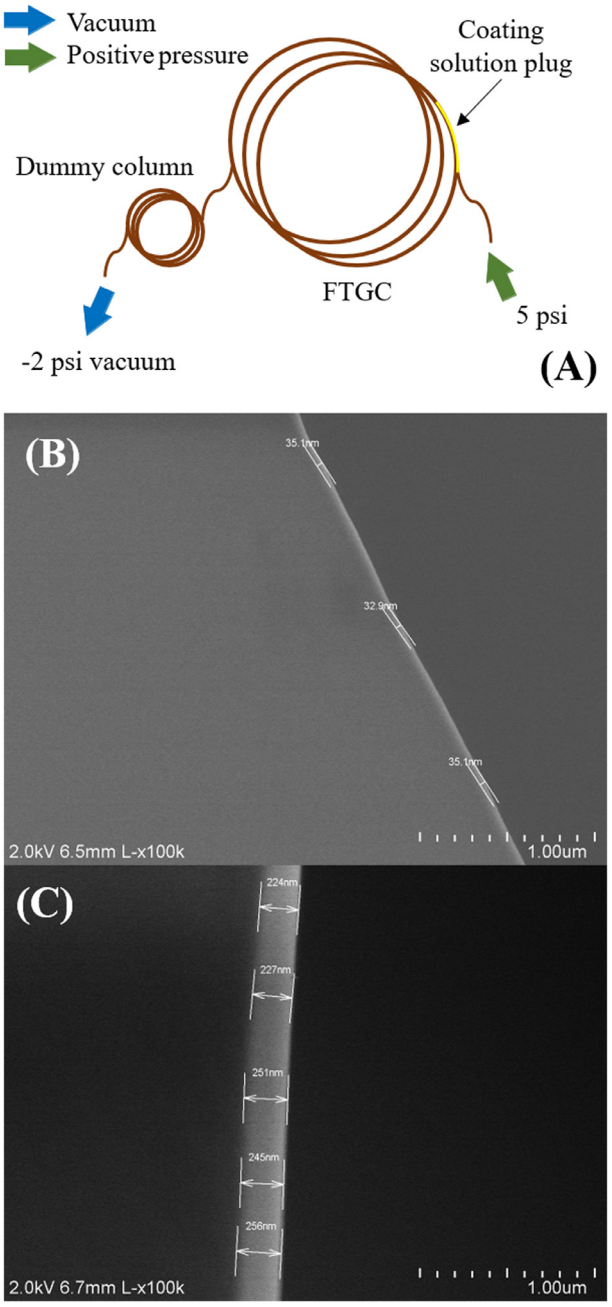

Fig. 2. (A) FTGC coating setup. The column was dynamically coated by partially filling with a coating solution plug and subsequently pushing the mixture out with a pressure of 5 psi. While pushing the solution out, a vacuum pressure of −2 psi was applied to the outlet to vaporize the solvent. (B) SEM image close to the column inlet with a film thickness of 34 nm. (C) SEM image close to the column outlet with a film thickness of 241 nm.

Table 2
Simulated retention times (RTs) and full widths at half maxima (FWHMs) for C_8–C_{15} in forward and backward modes. RTs and FWHMs for a uniform coating thickness are also provided for reference. The temperature was ramped from 40 °C at a rate of 30 °C/min with a head pressure of 3.45 psi. Column length was 5 m. All values are provided in minutes. Additional analysis is provided in Table 3.

	RT_{fwd}	$FWHM_{fwd}$	RT_{bkwd}	$FWHM_{bkwd}$	RT_{uni}	$FWHM_{uni}$
C_8	0.460	0.0382	0.439	0.0684	0.449	0.0519
C_9	0.731	0.0473	0.697	0.0995	0.714	0.0704
C_{10}	1.157	0.0574	1.113	0.1296	1.136	0.0885
C_{11}	1.639	0.0656	1.560	0.1487	1.615	0.1005
C_{12}	2.106	0.0713	2.055	0.1584	2.082	0.1073
C_{13}	2.591	0.0763	2.541	0.1640	2.568	0.1120
C_{14}	3.050	0.0807	3.001	0.1679	3.027	0.1158
C_{15}	3.460	0.0842	3.411	0.1708	3.437	0.1186

Table 3
Simulated resolutions (R) between adjacent peaks for C_8–C_{15} in forward and backward modes and for uniform thickness. Forward mode resolutions are all larger than backward mode and uniform thickness resolutions. The difference in resolution is defined as $R_{diff} = R_{fwd}$-R_{bkwd}.

	R_{fwd}	R_{bkwd}	R_{diff}	R_{uni}
C_8/C_9	3.744	1.814	1.930	2.554
C_9/C_{10}	4.808	2.147	2.661	3.133
C_{10}/C_{11}	4.619	2.020	2.599	2.992
C_{11}/C_{12}	4.024	1.787	2.237	2.647
C_{12}/C_{13}	3.884	1.779	2.105	2.615
C_{13}/C_{14}	3.448	1.634	1.814	2.379
C_{14}/C_{15}	2.932	1.429	1.503	2.065
PC	27.459	12.610	–	18.385

5. Results and discussion

5.1. Commercial column control

A Restek RTX-5 column (see the Materials section in Experimental) was used for separation of C_7–C_{16} alkanes in forward and backward modes as a control, with no difference in separation expected (separation conditions provided in Table 1). *p*-values for retention times and FWHMs (over 5 runs) were calculated using a paired Student's *t*-test and converting the resulting *T*-score to a *p*-value. Significance was taken at $p = 0.05$; no significant differences between forward and backward modes were observed for any analyte peak (see Section S4 – Control experiment using a Restek RTX-5 column in Supporting Information). Similarly, no significant differences between forward and backward modes were observed for C_7–C_{15} when a 5 m long Agilent DB-1MS column (data not shown) was used.

5.2. Stationary phase characterization

To characterize the thickness of the stationary phase, the FTGC was first frozen in liquid nitrogen and several pieces were scored off. Scanning electron microscopy (SEM) images were taken close to the column inlet (thinner film) and outlet (thicker film). Fig. 2(B) and (C) show that the film thickness increases from 34 nm to 241 nm from the inlet to the outlet, a gradient of approximately 41 nm/m. The uniform thickness column was also characterized at both the inlet and outlet with a film thickness of 131 nm at both column ends (see Section S5).

5.3. Peak focusing on alkane mixture

The FTGC's peak focusing capabilities were evaluated by separation of a C_7–C_{16} alkane mixture. 0.025 µL of liquid was used for injection at a split ratio of 5:1. The same separation conditions were used for forward mode, the uniform thickness column, and backward mode (denoted as "identical parameters backward mode", see Table 1 – alkane mixture). Example chromatograms are shown in Fig. 3.

Table 4
p-values between forward mode and uniform thickness, identical parameters (IP) backward, and equal time (ET) backward modes for C_7 to C_{16} alkanes separation. Significance is taken at $p = 0.05$. All *p*-values are significant between forward and IP backward mode, while *p*-values for C_7–C_{13} are significant for ET backward mode. Forward mode resolutions are significantly higher than uniform thickness resolutions up to C_{10}/C_{11}, while uniform thickness resolution is significantly higher for C_{15}/C_{16}.

Alkane pair	*p*-values		
	IP	ET	Uniform
C_7/C_8	0.001	9.77e−6	1.20e−4
C_8/C_9	5.27e−4	5.46e−5	1.18e−5
C_9/C_{10}	5.08e−4	1.39e−4	4.06e−5
C_{10}/C_{11}	1.27e−4	2.79e−4	0.046
C_{11}/C_{12}	7.38e−5	9.6e−4	0.585
C_{12}/C_{13}	5.35e−5	0.023	0.244
C_{13}/C_{14}	3.28e−6	0.146	0.358
C_{14}/C_{15}	2.80e−5	0.359	0.074
C_{15}/C_{16}	7.24e−5	0.430	0.006

Fig. 4 shows that analyte peaks in forward mode, for the uniform thickness column, and in identical parameters backward mode elute at different times, which is consistent with simulation (Table 2). This is due to the fact that separation conditions for a given analyte are different between the two modes, which in turn are different from the uniform thickness column. In forward mode, the analyte is first exposed to the thinner film at low temperatures before reaching the thicker film at high temperatures, exactly opposite of what the analyte experiences in backward mode. In the uniform thickness column, analytes experience the same film thickness at all temperatures. As a result, retention times for analytes in these two modes and in the uniform column are different and peak full widths at half maxima (FWHMs) are not directly comparable when assessing column performance. Instead, resolutions between adjacent peaks (*e.g.*, C_7 and C_8, C_8 and C_9, *etc.*) are used to analyze separation performance. Resolutions in identical parameters backward mode and for the uniform column are subtracted from corresponding resolutions in forward mode; the resolution differences (*i.e.*, $R_{forward} - R_{identical\ parameters\ backward}$ or $R_{forward} - R_{uniform}$) between all adjacent peak pairs (averaged over 5 runs) are plotted in Fig. 4. p-values for resolution difference are calculated using a paired Student's *t*-test (for 5 runs in forward and identical parameters backward modes and for the uniform column) and converting the resulting *T*-score to a *p*-value (see Table 4). Significance is taken at $p = 0.05$, showing that forward mode has significantly higher resolution between all pairs of adjacent peaks when compared to identical parameters backward mode. This is corroborated by simulation (Table 3), which also demonstrates higher resolutions in forward mode, meaning that in the same time interval, forward mode can contain more peaks than backward mode. Uniform thickness column resolutions are lower than forward mode resolutions up to C_{10}/C_{11}, but uniform resolution is higher for the C_{15}/C_{16} pair. Analysis of overall performance is provided below.

To further account for the discrepancy between retention times, a second set of chromatograms was obtained by lowering the backward mode ramping rate to ensure that C_{16} (the last eluted analyte) eluted at the same time as in forward mode (this is

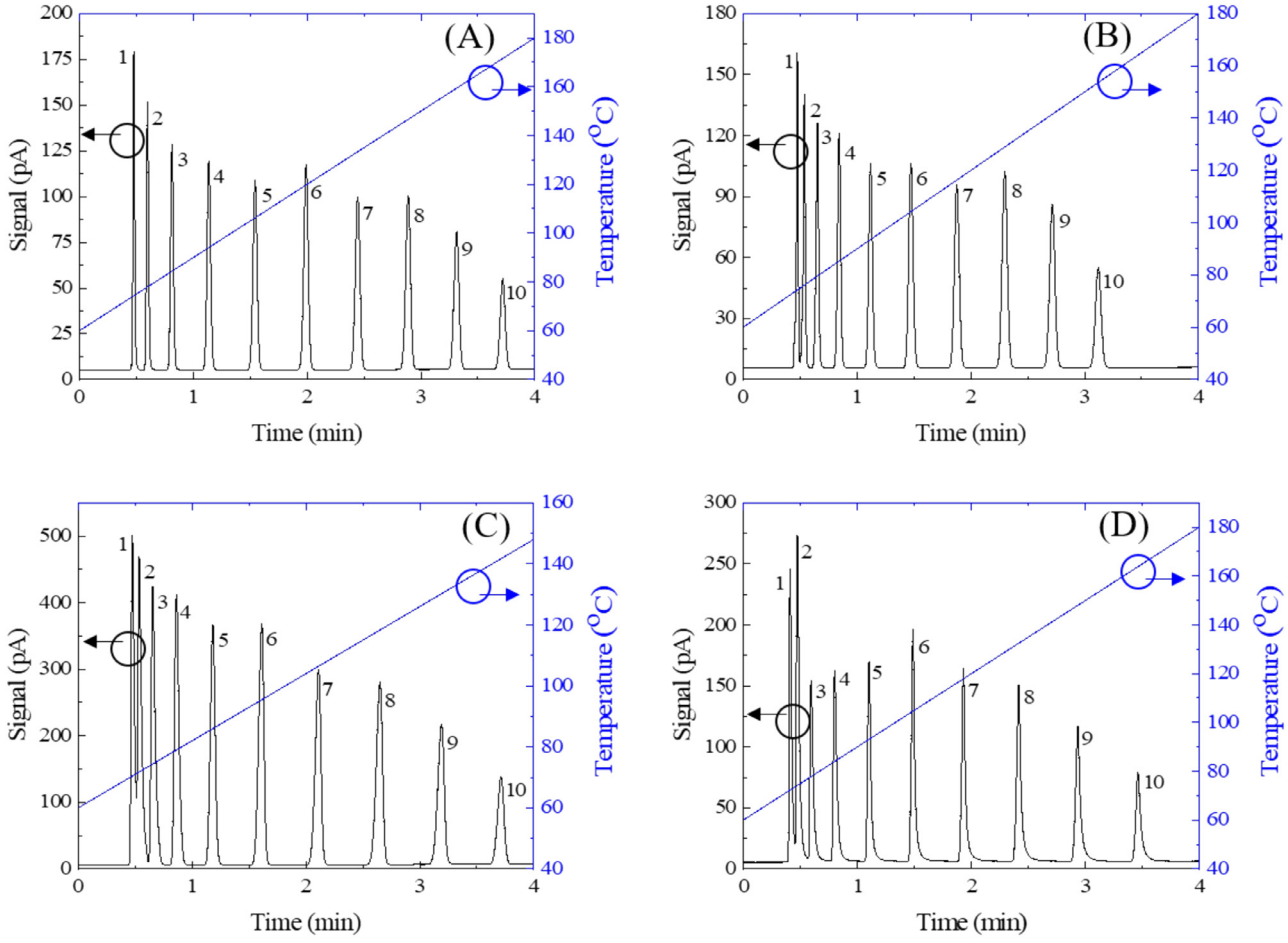

Fig. 3. Separation of a C_7–C_{16} alkane mixture in forward (A), identical parameters backward (B), and equal time backward (C) modes, and using a uniform thickness column (D). 0.025 µL of mixture liquid was injected into the injection portable for an Agilent 6890 benchtop GC. Carrier gas head pressure: 3.45 psi (2.7 mL/min at 60 °C).

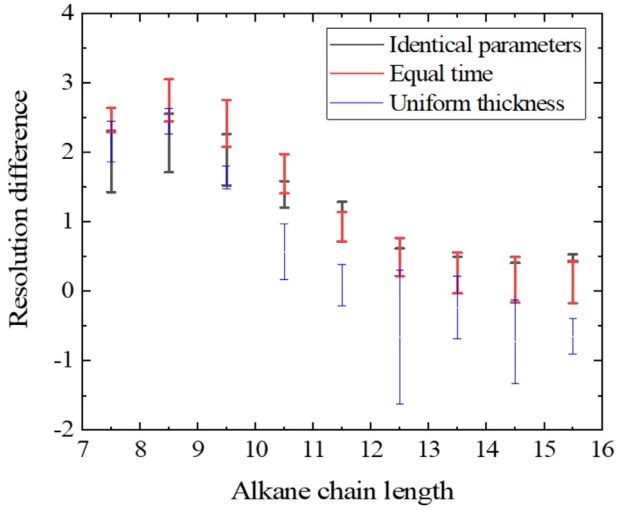

Fig. 4. Resolution differences between forward and identical parameters and equal time backward modes, and a uniform thickness column for C_7–C_{16} alkanes.

denoted as "equal time backward mode", see Table 1 – separation conditions, Fig. 3 – chromatograms, Fig. 4 – resolution differences, Table 4 – *p*-values). Again, forward mode provides significantly higher resolution for alkane pairs between C_7 and C_{13} (results obtained from 5 runs), but performs similarly to equal time backward mode for C_{13}–C_{16}. While forward mode does not outperform equal time backward mode (or the uniform thickness column) for all *local* resolutions (*i.e.*, between adjacent alkane pairs), forward mode has a significantly higher peak capacity (PC), defined as the sum over all resolutions (Table 5), compared to all other modes. Analysis of the focusing rate, defined as

$$FR = \frac{PC_{forward} - PC_{backward/uniform}}{PC_{backward/uniform}}, \tag{24}$$

shows that forward mode demonstrates overall focusing rates of approximately 11.7%, 26.8%, and 29.8% when compared with the

Table 5
Peak capacities, *p*-values, and focusing rates between forward mode and identical parameters (IP) and equal time (ET) backward modes, and uniform thickness for C_7–C_{16} alkanes separation in Fig. 3. Significance is taken at $p = 0.05$. Peak capacity in forward mode is significantly higher than peak capacities in all other modes.

Forward peak capacity	49.34 ± 0.841
Backward peak capacity (IP)	38.90 ± 0.831
p-value (IP)	1.73e−4
Focusing rate (IP)	26.84%
Backward peak capacity (ET)	38.02 ± 2.400
p-value (ET)	4.62e−4
Focusing rate (ET)	29.76%
Uniform peak capacity	44.18 ± 0.483
p-value (uniform)	1.63e−4
Focusing rate (uniform)	11.67%

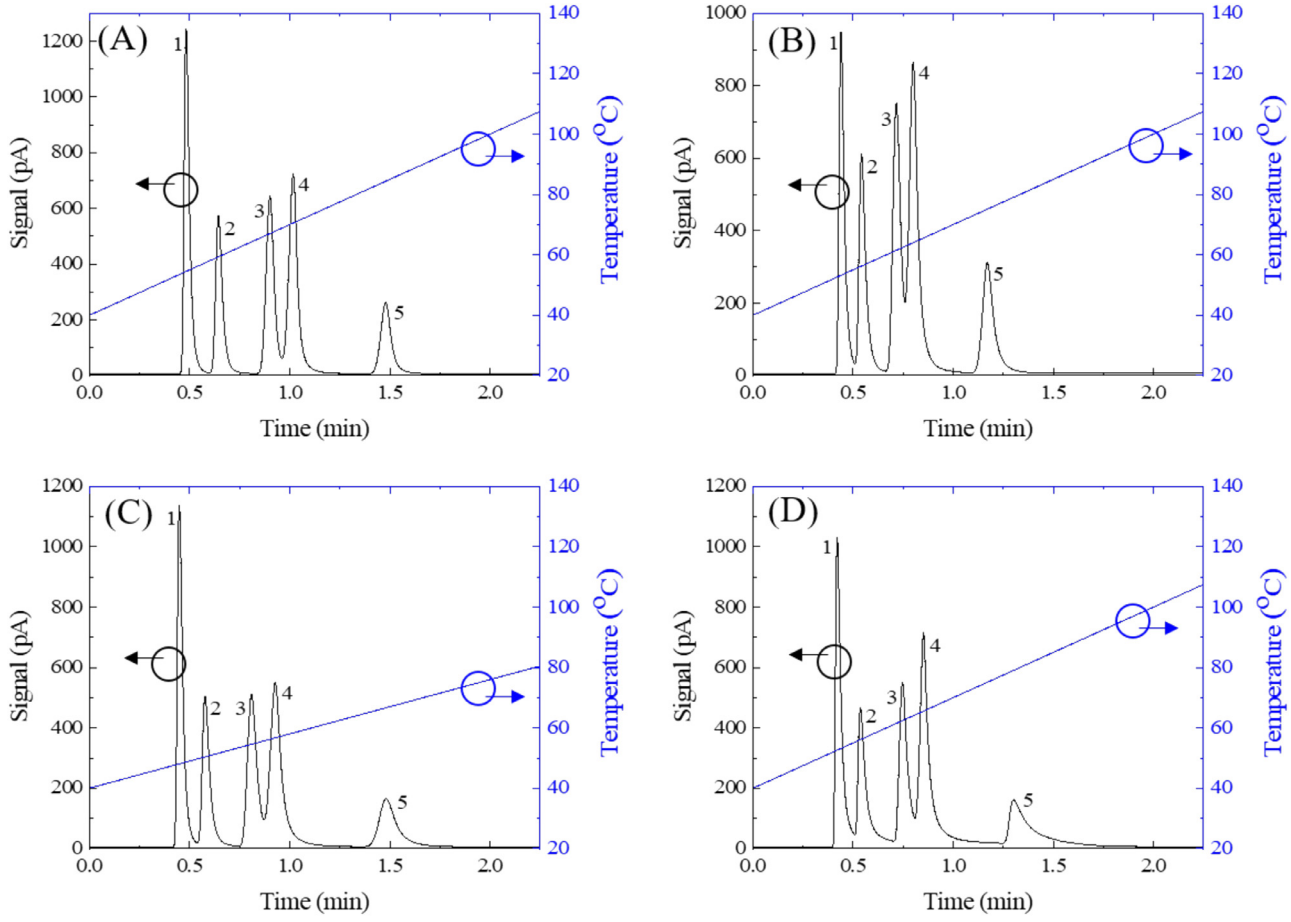

Fig. 5. Separation of an aromatics mixture in forward (A), identical parameters (B), and equal time backward (C) modes, and using a uniform thickness column (D). 0.025 µL of mixture liquid was injected with a carrier gas head pressure of 3.45 psi (2.9 mL/min at 45 °C). 1. Benzene (B); 2. Toluene (T); 3. Ethylbenzene (E); 4. o-Xylene (X); 5. 1,3-dichlorobenzene (DCB).

Table 6
p-values between forward mode and uniform thickness, identical parameters backward (IP), and equal time backward (ET) modes for aromatics separation. See Fig. 5 for elution order and abbreviations. Significance is taken at $p = 0.05$. All *p*-values show significantly improved resolution in forward mode.

p-values	*p*-values (IP)	*p*-values (ET)	*p*-values (Uniform)
B/T	3.08e−7	5.56e−7	1.83e−5
T/E	3.84e−7	9.28e−7	4.20e−6
E/X	9.32e−6	8.28e−5	0.012
X/DCB	5.95e−6	2.06e−5	2.28e−5

uniform thickness column, identical parameters backward mode, and equal time backward mode, respectively.

5.4. Peak focusing on aromatics mixture

FTGC peak focusing was also analyzed on separation of an aromatics mixture containing benzene, toluene, ethylbenzene, o-xylene, and 1,3-dichlorobenzene. 0.025 µL of mixture liquid was injected at a split ratio of 5:1 (separation conditions provided in Table 1 – aromatics mixture). Example chromatograms are shown in Fig. 5 and resolution differences are shown in Fig. 6. Local resolution difference *p*-values (calculated from 5 runs) are provided in Table 6. Peak capacities, *p*-values, and focusing rates are provided in Table 7, showing that forward mode has significantly higher peak capacity compared to all other modes. Thus, regardless of whether separation parameters are kept constant (and analytes

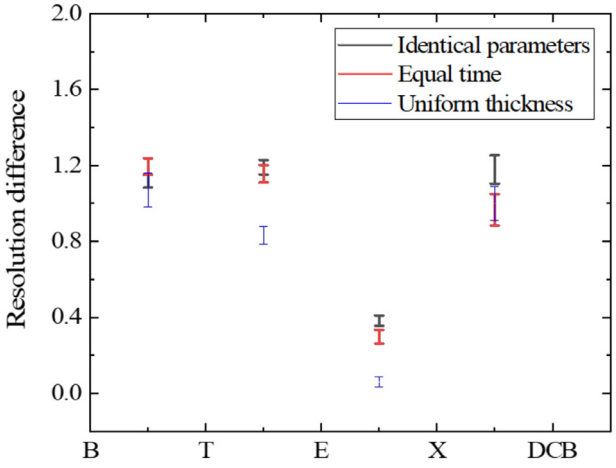

Fig. 6. Resolution differences between forward and identical parameters backward and equal time backward modes, and a uniform thickness column for aromatics separation. Resolution difference is always positive, indicating that separation in forward mode is always better than separation in all other modes.

elute faster in identical parameters backward mode) or changed to ensure that the last compound elutes at the same time (in forward and equal time backward modes), separation performance in forward mode is always better than in either backward mode. Forward mode also outperforms the uniform thickness column, demonstrating a focusing rate of 28.2% (Table 7). Thus, overall,

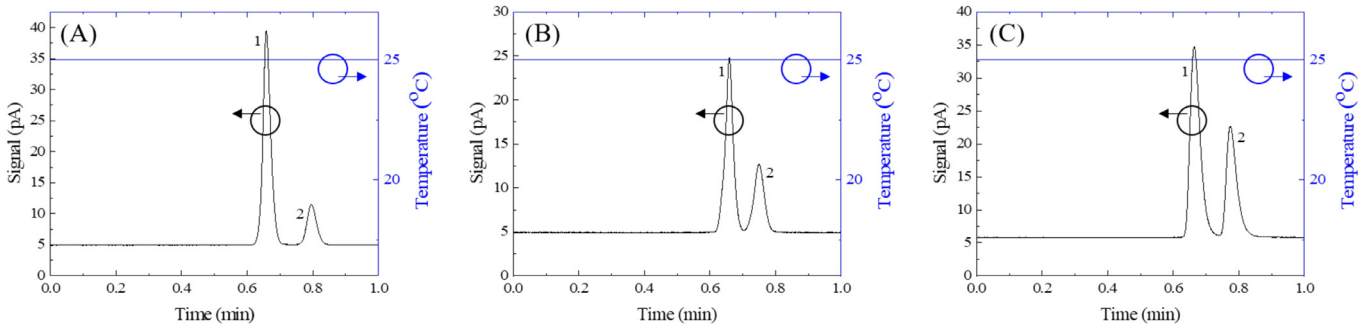

Fig. 7. Room temperature (26 °C) isothermal separation of C_5 and C_6 in forward mode (A), identical parameters backward (B) mode, and using a uniform thickness column (C). 0.2 µL of vapor obtained from the headspace of a C_5 and C_6 mixture was injected using a carrier gas head pressure of 2.2 psi (2 mL/min).

Table 7
Peak capacities, *p*-values, and focusing rates between forward mode and identical parameters (IP) and equal time (ET) backward modes, and uniform thickness for aromatics separation in Fig. 5. Significance is taken at $p = 0.05$. Separation in forward mode is significantly better than separation all other modes.

Forward peak capacity	13.47 ± 0.089
Backward peak capacity (IP)	9.59 ± 0.060
p-value (IP)	1.60e−7
Focusing rate (IP)	40.35%
Backward peak capacity (ET)	9.85 ± 0.093
p-value (ET)	1.56e−6
Focusing rate (ET)	36.73%
Uniform peak capacity	10.50 ± 0.146
p-value (uniform)	1.13e−5
Focusing rate (uniform)	28.22%

Table 9
Resolutions, *p*-values, and focusing rates for forward mode, backward mode, and uniform thickness for room temperature (26 °C) C_5 and C_6 separation. Significance is taken at $p = 0.05$.

Forward resolution	2.97 ± 0.140
Backward resolution	1.85 ± 0.055
p-value (backward)	1.17e−4
Focusing rate (backward)	60.4%
Uniform resolution	2.12 ± 0.049
p-value (uniform)	4.87e−4
Focusing rate (uniform)	40.2%

forward mode (i.e., a positive film thickness gradient) demonstrates the ability to improve separation peak capacity.

5.5. Temperature ramping effects

To demonstrate how temperature ramping rate affects peak focusing, separation of C_7–C_{10} with four different ramping rates (0, 10, 20, and 30 °C/min, ramped from 60 °C without holding) was performed in forward mode, identical parameters backward mode, and using the uniform thickness column. The head pressure was 3.45 psi (2.7 mL/min at 60 °C) and the split ratio was 15:1 for all separations (0.025 µL mixture liquid injection). The void time was measured by methane injection and was found to be 0.36 min for all ramping rates. Resolutions and focusing rates for each temperature profile are provided in Table 8 (values provided as averages over 5 runs). In forward mode, at higher temperature ramping rates, analytes encounter relatively higher temperatures by the time they reach the thicker stationary phase closer to the column outlet. The analyte thus spends less time in the thicker film and peak broadening is reduced. In backward mode, analytes first encounter the thicker stationary phase at lower temperatures before flowing to the thinner stationary phase at higher temperatures. Peak broadening from low thickness stationary phases is already low; therefore, the overall decrease in peak broadening due to increased temperature is lower in backward mode. Thus, the focusing rate increases with increased temperature ramping rate, up to 61.9% comparing forward and backward modes and 68.1% comparing forward mode and uniform thickness at a rate of 30 °C/min.

5.6. Focusing for high volatility compounds

Unlike NTGS, an FTGC gradient is capable of focusing peaks at low temperatures (as long as said peaks are reasonably retained at these temperatures), where a temperature gradient is difficult to generate. To demonstrate this, room temperature isothermal separation (Table 1) of C_5 and C_6 was performed (Fig. 7). Resolutions, p-values, and focusing rates are provided in Table 9 (values averaged over 5 runs). A focusing rate of 40.2% was achieved with an average forward mode resolution of 2.97 and uniform thickness resolution of 2.12. Note that for NTGS, the same peak focusing effect for high volatility compounds is difficult to achieve since only small temperature gradients can be generated at low operating temperatures.

Table 8
Resolutions (R), peak capacities (PC), and focusing rates for forward mode, identical parameters backward mode, and uniform thickness for C_7–C_{10} separation at various temperature ramping rates. The initial temperature was 60 °C for all separations and the carrier gas head pressure was 3.45 psi (2.7 mL/min at 60 °C). 0.025 µL of mixture liquid was injected using a split ratio of 15:1.

Ramping rate (°C/min)	$R_{fwd}/R_{bkwd}/R_{uni}$ (C_7/C_8)	$R_{fwd}/R_{bkwd}/R_{uni}$ (C_8/C_9)	$R_{fwd}/R_{bkwd}/R_{uni}$ (C_9/C_{10})	$PC_{fwd}/PC_{bkwd}/PC_{uni}$	Focusing rate (bkwd/uni)
0	4.59/3.40/2.74	5.86/4.68/4.86	6.73/5.68/7.43	17.18/13.76/15.02	24.85%/14.36%
10	4.60/3.18/2.73	5.80/4.40/4.42	6.65/5.38/6.69	17.05/12.96/13.84	31.56%/21.63%
20	4.43/2.86/2.53	5.51/3.94/4.02	6.39/4.88/5.77	16.32/11.68/12.32	39.73%/37.25%
30	4.01/2.14/1.84	5.30/3.16/2.85	6.11/4.22/4.48	15.41/9.52/9.17	61.87%/68.09%

6. Conclusion

Development and evaluation of a stationary phase thickness gradient column technique that enables peak focusing has been detailed herein. Experimental results were corroborated by theoretical analysis and simulation, showing increased separation performance of various compounds in forward mode, including focused separation of high volatility compounds at room temperature. Compared to NTGS, the FTGC has advantages in larger applicable temperature and compound volatility ranges, simple operation without accessories, less dependence on ambient conditions, and greater compactness. This stationary phase thickness gradient technique can be facilely applied to wide-ranging GC applications and can be used for stationary phases of any materials or thicknesses, provided only that a gradient can be generated. Furthermore, it is applicable to both regular circular cross-sectioned capillary columns and rectangular cross-sectioned microfabricated columns (for additional information, see Section S6 - Film thickness gradient microcolumn in Supporting Information). Future work may target improving FTGC flexibility by combining this technique with NTGS, allowing for online tuning of peak focusing and greater improvement of GC separation performance.

Declaration of Competing Interest

The authors declare no conflict of interest.

CRediT authorship contribution statement

Maxwell Wei-Hao Li: Conceptualization, Investigation, Methodology, Formal analysis, Data curation, Writing - original draft. **Hongbo Zhu:** Conceptualization, Investigation, Methodology, Formal analysis, Data curation, Writing - original draft. **Menglian Zhou:** Methodology, Formal analysis, Data curation, Writing - original draft. **Jinyan She:** Methodology, Writing - original draft. **Ziqi Li:** Methodology. **Katsuo Kurabayashi:** Data curation, Writing - original draft. **Xudong Fan:** Conceptualization, Investigation, Formal analysis, Data curation, Writing - original draft.

Acknowledgments

The research is based upon work supported by the Office of the Director of National Intelligence (ODNI), Intelligence Advanced Research Projects Activity (IARPA), via IARPA FA8650-17-C-9106 and by National Institute for Occupational Safety and Health (NIOSH) via R01 OH011082-01A1. The views and conclusions contained herein are those of the authors and should not be interpreted as necessarily representing the official policies or endorsements, either expressed or implied, of the ODNI, IARPA, or the U.S. Government. The U.S. Government is authorized to reproduce and distribute reprints for Governmental purposes notwithstanding any copyright annotation thereon.

Supplementary materials

Supplementary material associated with this article can be found, in the online version, at doi:10.1016/j.chroma.2019.460737.

References

[1] D.V. Gough, H.D. Bahaghighat, R.E. Synovec, Column selection approach to achieve a high peak capacity in comprehensive three-dimensional gas chromatography, Talanta 195 (2019) 822–829.
[2] Y.V. Patrushev, V.N. Sidelnikov, Selection of the porous layer open tubular columns for separation of light components in comprehensive two-dimensional gas chromatography, J. Chromatogr. A 1579 (2018) 83–88.
[3] H. Nan, J.L. Anderson, Ionic liquid stationary phases for multidimensional gas chromatography, TrAC Trends Anal. Chem. 105 (2018) 367–379.
[4] J.V. Seeley, C.T. Bates, J.D. McCurry, S.K. Seeley, Stationary phase selection and comprehensive two-dimensional gas chromatographic analysis of trace biodiesel in petroleum-based fuel, J. Chromatogr. A 1226 (2012) 103–109.
[5] M. Giardina, J.D. McCurry, Comparison of temperature programmable split/splitless and cool on-column inlets for the determination of glycerol and glycerides in biodiesel by gas chromatography with flame ionization detection, J. Chromatogr. Sci. 54 (2016) 683–688.
[6] N.H. Snow, Temperature Programmed GC: Why are All Those Peaks so sharp?, LCGC North America, 2019 [Online early access].
[7] L.M. Blumberg, Temperature-Programmed Gas Chromatography, John Wiley & Sons, 2010.
[8] S. Reidy, D. George, M. Agah, R. Sacks, Temperature-Programmed GC using silicon microfabricated columns with integrated heaters and temperature sensors, Anal. Chem. 79 (2007) 2911–2917.
[9] M. Agah, J.A. Potkay, G. Lambertus, R. Sacks, K.D. Wise, High-performance temperature-programmed microfabricated gas chromatography columns, J. Microelectromech. Syst. 14 (2005) 1039–1050.
[10] Restek's PLOT Column Family – The Benchmark for Performance. https://www.restek.com/Technical-Resources/Technical-Library/Petroleum-Petrochemical/Restek-s-PLOT-Column-Family-PCSS1163G-UNV.
[11] Z.H. Ji, R.E. Majors, E.J. Guthrie, Porous layer open-tubular capillary columns: preparations, applications and future directions, J. Chromatogr. 842 (1999) 115–142.
[12] A.A. Zhukhovitskii, O.V. Zolotareva, V.A. Sokolov, N.M. Turkel'taub, New method of chromatographic analysis, Dokl. Akad. Nauk SSSR 77 (1951) 435–438.
[13] L.M. Blumberg, Limits of resolution and speed of analysis in linear chromatography with and without focusing, Chromatographia 39 (1994) 719–728.
[14] J.A. Contreras, A. Wang, A.L. Rockwood, H.D. Tolley, M.L. Lee, Dynamic thermal gradient gas chromatography, J. Chromatogr. 1302 (2013) 143–151.
[15] J.A. Contreras, A.L. Rockwood, H.D. Tolley, M.L Lee, Peak sweeping and gating using thermal gradient gas chromatography, J. Chromatogr. 1278 (2013) 160–165.
[16] H.D. Tolley, S.E. Tolley, A. Wang, M.L. Lee, Moving thermal gradients in gas chromatography, J. Chromatogr. 1374 (2014) 189–198.
[17] P. Boeker, J. Leppert, Flow field thermal gradient gas chromatography, Anal. Chem. 87 (2015) 9033–9041.
[18] A. Wang, S. Hynynen, A.R. Hawkins, S.E. Tolley, H.D. Tolley, M.L. Lee, Axial thermal gradients in microchip gas chromatography, J. Chromatogr. 1374 (2014) 216–223.
[19] A. Ghosh, J.E. Johnson, J.G. Nuss, B.A. Stark, A.R. Hawkins, L.T. Tolley, B.D. Iverson, H.D. Tolley, M.L. Lee, Extending the upper temperature range of gas chromatography with all-silicon microchip columns using a heater/clamp assembly, J. Chromatogr. 1517 (2017) 134–141.
[20] F. Aldaeus, Y. Thewalim, A. Colmsjo, Prediction of retention times and peak widths in temperature-programmed gas chromatography using the finite element method, J. Chromatogr. A 1216 (2009) 134–139.
[21] K. Bartle, Film thickness of dynamically coated open-tubular glass columns for gas chromatography, Anal. Chem. 45 (1973) 1831–1836.
[22] F.R. Gonzalez, L.G. Gagliardi, Distribution coefficients of n-alkanes measured on wall-coated capillary columns, J. Chromatogr. A 879 (2000) 157–168.